

Designing Low-Concentration Propylene Carbonate-based Electrolyte by Manipulating Lithium⁺-Solvation Structure for Graphite Anode

Dichang Guan,^[a] Guorong Hu,^[a, b] Zhongdong Peng,^[a, b] Yanbing Cao,^[a, c] Zhanggen Gan,^[a] Xudong Zhang,^[a] and Ke Du^{*[a, c]}

We systematically study the correlation between Li⁺-solvation structure, interfacial stability, and electrochemical behavior in the system of graphite anode with low-concentration (0.5 M) propylene carbonate (PC)-based electrolyte (LCPE). 1,1,2,2-tetrafluoroethyl-2,2,3,3-tetrafluoropropylether (TTE) [or 1,1,2,2-tetrafluoroethyl-2,2,2-trifluoroethyl ether (HFE)] is used to manipulate the solvation structures of Li⁺ in the LCPEs. Varying Li⁺-solvation structures are realized by changing the volume ratios of PC to TTE (or HFE) in the LCPEs. With the increase of

TTE (or HFE) dosages, the relative contents of LiF and Li_xPO_yF_z in SEI derived from PF₆⁻ increase, while the decomposition products of PC reduce. With enough TTE (or HFE) in the LCPE, the Li|graphite cell exhibits reversible (de)lithiation without PC co-intercalation and continuous electrolyte decomposition due to the shield of a compact SEI rich in LiF and Li_xPO_yF_z. Our work proves it is practicable to achieve LiF-riched SEIs on graphite anodes and realize reversible (de)lithiation in LCPEs by regulating the Li⁺-solvation structures with inert cosolvents.

Introduction

In the initial exploration of applying carbonates in the electrolytes for lithium-ion batteries (LIBs), propylene carbonate (PC) rather than ethylene carbonate (EC) was favored due to its wide liquid range (-48.8°C – 242°C), high dielectric constant ($\epsilon = 64.92$) and good oxidation stability ($>4\text{ V}$).^[1,2] Unfortunately, graphite, the most optimal anode, failed to (de)lithiation reversibly due to the co-intercalation of PC molecules and continuous decomposition of electrolytes in PC-based electrolyte. Extensive attempts have been made to prevent the exfoliation of graphite and realize reversible (de)intercalation of Li⁺ within the graphite in PC-based electrolytes. The common methods can be categorized as follows: (1) adding film-forming additives to generate uniform solid electrolyte interphase (SEI) on the graphite anode.^[3–6] (2) coating graphite with inert materials to prevent the direct contact of electrolyte with graphite.^[7–9] (3) increasing the lithium salt concentration to regulate the Li⁺-solvation structure.^[10–13]

In 2003, Jeong et al. first reported reversible (de)intercalation of Li⁺ within graphite anode in a concentrated electrolyte consisting of 2.72 M LiN(SO₂C₂F₅)₂ (LiBETI) in pure PC.^[10] Moreover, Nie et al. further demonstrated that the solution structure dominated by contact ion pairs [Li⁺(PC)₃PF₆] in concentrated PC-based electrolyte (3–3.5 M) results in a LiF-rich SEI on the surface of graphite anode, which inhibits PC co-intercalation and electrolyte decomposition.^[12] However, the high viscosities of high-concentration PC-based electrolytes seriously deteriorate the cycle and rate performances of LIBs. Besides, the high costs of concentrated electrolytes induced by the large amount expensive lithium salts also impede their large-scale applications.

In our recent work, we reported a low-concentration electrolyte containing 0.4 M LiPF₆ in the ternary mixtures of EC, dimethyl carbonate (DMC), and 1,1,2,2-tetrafluoroethyl-2,2,3,3-tetrafluoropropyl ether (TTE).^[14] We proved that the presence of TTE in the low-concentration electrolyte can change the Li⁺-solvation structure prominently. The unique solution structure leads to enhanced oxidation stability of the low-concentration electrolyte and conduces to forming a LiF-rich SEI on the cathode. Inspired by this, we exploited a series of LCPEs containing only 0.5 M LiPF₆ in a mixture of PC and TTE or 1,1,2,2-Tetrafluoroethyl-2,2,2-trifluoroethyl ether (HFE) with different volume ratios. TTE (or HFE) was used to regulate the solution structure of the LCPEs just like we did before.^[14] It is unprecedented to achieve good compatibility between low-concentration PC-based electrolytes and graphite anodes, which provides new guidelines for developing PC-based electrolytes based on the Li⁺-solvation structure for graphite anodes.

[a] D. Guan, Prof. G. Hu, Prof. Z. Peng, Prof. Y. Cao, Z. Gan, X. Zhang, Prof. K. Du

School of Metallurgy and Environment
Central South University
Changsha, Hunan 410083, P. R. China
E-mail: duke22@csu.edu.cn

[b] Prof. G. Hu, Prof. Z. Peng
Hunan Provincial Key Laboratory of Nonferrous Value-added Metallurgy
Central South University
Changsha, Hunan 410083, P. R. China

[c] Prof. Y. Cao, Prof. K. Du
Engineering Research Center of the Ministry of Education for Advanced
Battery Materials
Central South University
Changsha, Hunan 410083, P. R. China

 Supporting information for this article is available on the WWW under
<https://doi.org/10.1002/batt.202200257>

Results and Discussion

The formula and identification for each electrolyte in the 0.5 M LiPF₆-PC/TTE system (05PT system) are listed in Table 1. In order to explore the variation of Li⁺-solvation structure with the introduction of TTE, Raman spectra for TTE, PC, PC+TTE (1:1, V/V), 0.5 M-PT11, 0.5 M-PT12, 0.5 M-PT13 and 0.5 M-PT14 were carried out. The Raman spectra of all solvents and electrolytes are shown from 500 to 900 cm⁻¹ (Figure 1a). The peaks at 712 cm⁻¹ and 724 cm⁻¹ can be attributed to free PC molecules and solvating PC molecules, respectively.^[10,15,16] With the addition of TTE, the relative intensities of the peaks related to free PC molecules keep decreasing while the peak intensities of solvating PC molecules keep increasing. It suggests that the

proportion of free-state PC molecules is reduced. Meanwhile, the relative intensities of the peaks related to PF₆⁻ at 742 cm⁻¹ keep increasing with the increase of TTE contents, which indicates the addition of TTE has a similar effect to increasing the concentration of lithium salt in PC-based electrolyte.^[17]

Figure 1(b and c) shows initial discharge-charge profiles of Li||graphite cells in the 05PT system. In the 0.5 M-PT10 electrolyte, the Li||graphite cell exhibits a long plateau near 0.8 V, corresponding to ceaseless solvent decomposition and continuous co-intercalation of PC during the initial discharge process. It is the typical discharge profile of graphite anode in PC-based electrolyte as mentioned in previous studies.^[6,10,18] With the addition of TTE, the Li||graphite cell in the 0.5 M-PT11 electrolyte also shows a long flat plateau near 0.8 V and has no charge capacity. It indicates that the decomposition of solvents and the intercalation of PC are not suppressed in the 0.5 M-PT11 electrolyte. It is noteworthy that the plateau of Li||graphite cell in the 0.5 M-PT11 electrolyte is slightly lower than that in the 0.5 M-PT10 electrolyte, which may be caused by the different Li⁺-solvation structures in the 0.5 M-PT10 and 0.5 M-PT11 electrolyte.^[12] With the further increase of TTE contents, the Li||graphite cells in the 0.5 M-PT12, 0.5 M-PT13, and 0.5 M-PT14 electrolyte all show several voltage plateaus below

Table 1. Electrolyte formulas of the 05PT system.

Electrolyte formula	ID
0.5 M LiPF ₆ -PC/TTE (1:0, V/V)	0.5 M-PT10
0.5 M LiPF ₆ -PC/TTE (1:1, V/V)	0.5 M-PT11
0.5 M LiPF ₆ -PC/TTE (1:2, V/V)	0.5 M-PT12
0.5 M LiPF ₆ -PC/TTE (1:3, V/V)	0.5 M-PT13
0.5 M LiPF ₆ -PC/TTE (1:4, V/V)	0.5 M-PT14

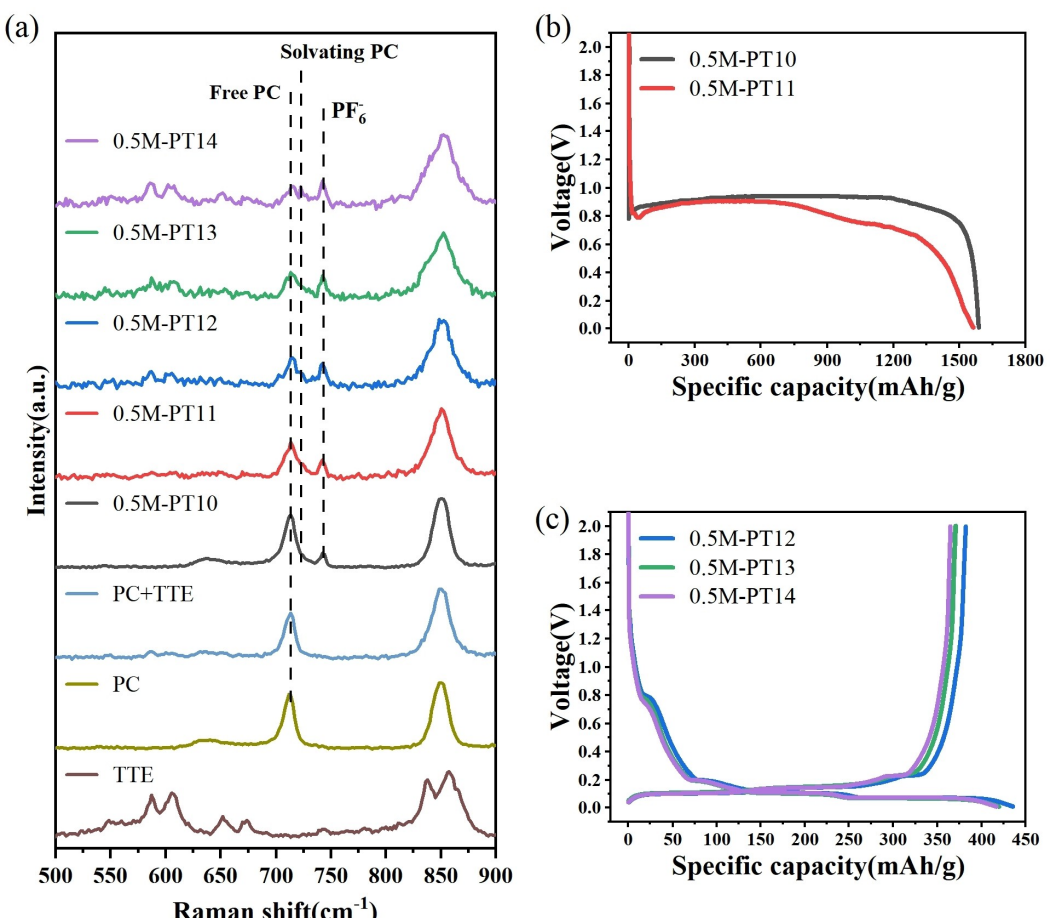


Figure 1. a) Raman spectra of TTE, PC, PC+TTE (1:1, V/V), 0.5 M-PT10, 0.5 M-PT11, 0.5 M-PT12, 0.5 M-PT13, and 0.5 M-PT14. b) Initial voltage profiles of Li||graphite cells in the 0.5 M-PT10 and 0.5 M-PT11 electrolyte at 0.1 C. c) Initial voltage profiles of Li||graphite cells in the 0.5 M-PT12, 0.5 M-PT13 and 0.5 M-PT14 electrolyte at 0.1 C.

~0.2 V, corresponding to the progressive formation of the multi-stage structure of Li_xC .^[10] And the initial Coulombic efficiencies of $\text{Li}||\text{graphite}$ cells in the 0.5 M-PT12, 0.5 M-PT13, and 0.5 M-PT14 electrolyte are 87.69%, 88.32%, and 89.11%, respectively. Hence, adding enough TTE in the LCPEs can restrain the co-intercalation of PC molecules and the decomposition of electrolytes.

The cyclic voltammograms of $\text{Li}||\text{graphite}$ cells in different electrolytes (Figure S1) confirm that the co-intercalation of PC molecules and decomposition of electrolytes are prevailing in the 0.5 M-PT10 and 0.5 M-PT11 electrolyte. However, reversible (de)lithiation is achieved in the 0.5 M-PT12, 0.5 M-PT13, and 0.5 M-PT14 electrolyte. The cathodic peaks near 0.8 V in the first cycle for the $\text{Li}||\text{graphite}$ cells in the 0.5 M-PT12, 0.5 M-PT13, and 0.5 M-PT14 electrolyte can be attributed to the reduction of PC to form SEIs. Besides, the cathodic peaks near 0.8 V disappear in the second and third cycles, suggesting effective SEIs are formed on the graphite anodes during the first cycle.

In order to investigate the exfoliation of graphite anodes after one cycle at 0.1 C in different electrolytes, the top-views of the graphite electrodes and the morphologies of graphite particles were observed by scanning electron microscope (SEM) (Figure 2a and b). Due to the co-intercalation of PC molecules in the 0.5 M-PT10 and 0.5 M-PT11 electrolyte, the graphite anodes after one cycle appear many huge cracks, and the graphite particles become fluffy and porous. More visually, the graphite anodes exfoliate extensively in the 0.5 M-PT10 and 0.5 M-PT11 electrolyte, as shown in the insets of Figure 2(a). The graphite anodes almost maintain their pristine morpholo-

gies after one cycle in the 0.5 M-PT12, 0.5 M-PT13, and 0.5 M-PT14 electrolyte. It demonstrates that the co-intercalation of PC molecules is successfully suppressed in the 0.5 M-PT12, 0.5 M-PT13, and 0.5 M-PT14 electrolyte.

The graphite structures after one cycle were further studied by Raman spectroscopy (Figure 2c). The peaks at 1350 cm^{-1} (D band) and 1580 cm^{-1} (G band) are assigned to the disordered structure and the crystalline lattice of graphite, respectively.^[19] The intensity ratio of the D and G band (I_D/I_G) can be used to estimate the degree of defectiveness in graphite.^[20] The I_D/I_G of the graphite anode increases from 0.24 for the pristine graphite anode to 0.87 and 0.69 for the graphite anode after one cycle in the 0.5 M-PT10 and 0.5 M-PT11 electrolyte, respectively. It indicates the graphite anodes suffered severe structural deteriorations due to the co-intercalation of PC molecules. The I_D/I_G of the graphite anodes after one cycle in the 0.5 M-PT12, 0.5 M-PT13, and 0.5 M-PT14 electrolyte are 0.33, 0.33, and 0.24, respectively. It suggests that the graphitization degrees of graphite anodes decrease slightly in the 0.5 M-PT12, 0.5 M-PT13, and 0.5 M-PT14 electrolyte.

X-ray photoelectron spectroscopy (XPS) was used to investigate the SEI components on the graphite anodes after one cycle in different electrolytes. There are similar element peaks in the XPS survey spectra of graphite anodes after one cycle in the 05PT system (Figure S2a and b). As the TTE contents increases, the atomic ratios of C and O elements on the graphite anodes surface show a general decrease trend (Figure S2c). The strong signals of LiC_x (Figure 3) in the C1s spectra indicate that the SEIs formed on the graphite anodes

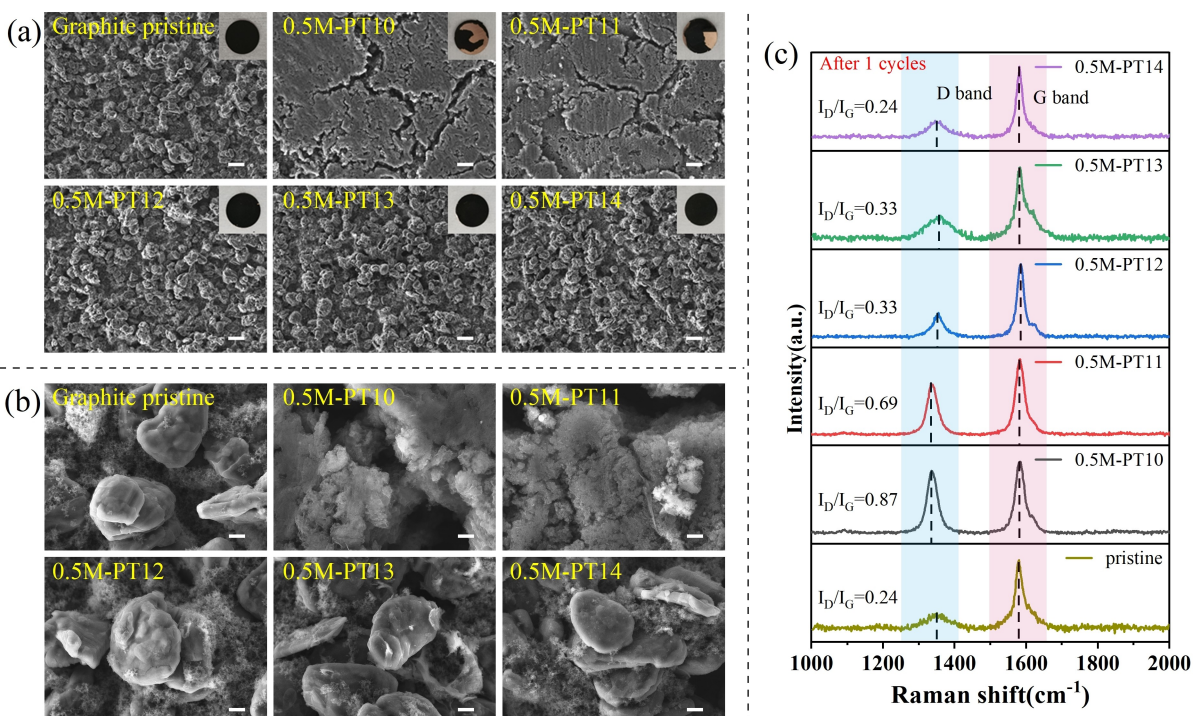


Figure 2. a) Top-views of the graphite anodes and b) morphologies of the graphite particles after one cycle in the 0.5 M-PT10, 0.5 M-PT11, 0.5 M-PT12, 0.5 M-PT13, and 0.5 M-PT14 electrolyte. Scale bars, a) $20 \mu\text{m}$ and b) $2 \mu\text{m}$. c) Raman spectra of the pristine and cycled graphite anodes in the 0.5 M-PT10, 0.5 M-PT11, 0.5 M-PT12, 0.5 M-PT13, and 0.5 M-PT14 electrolyte after one cycle.

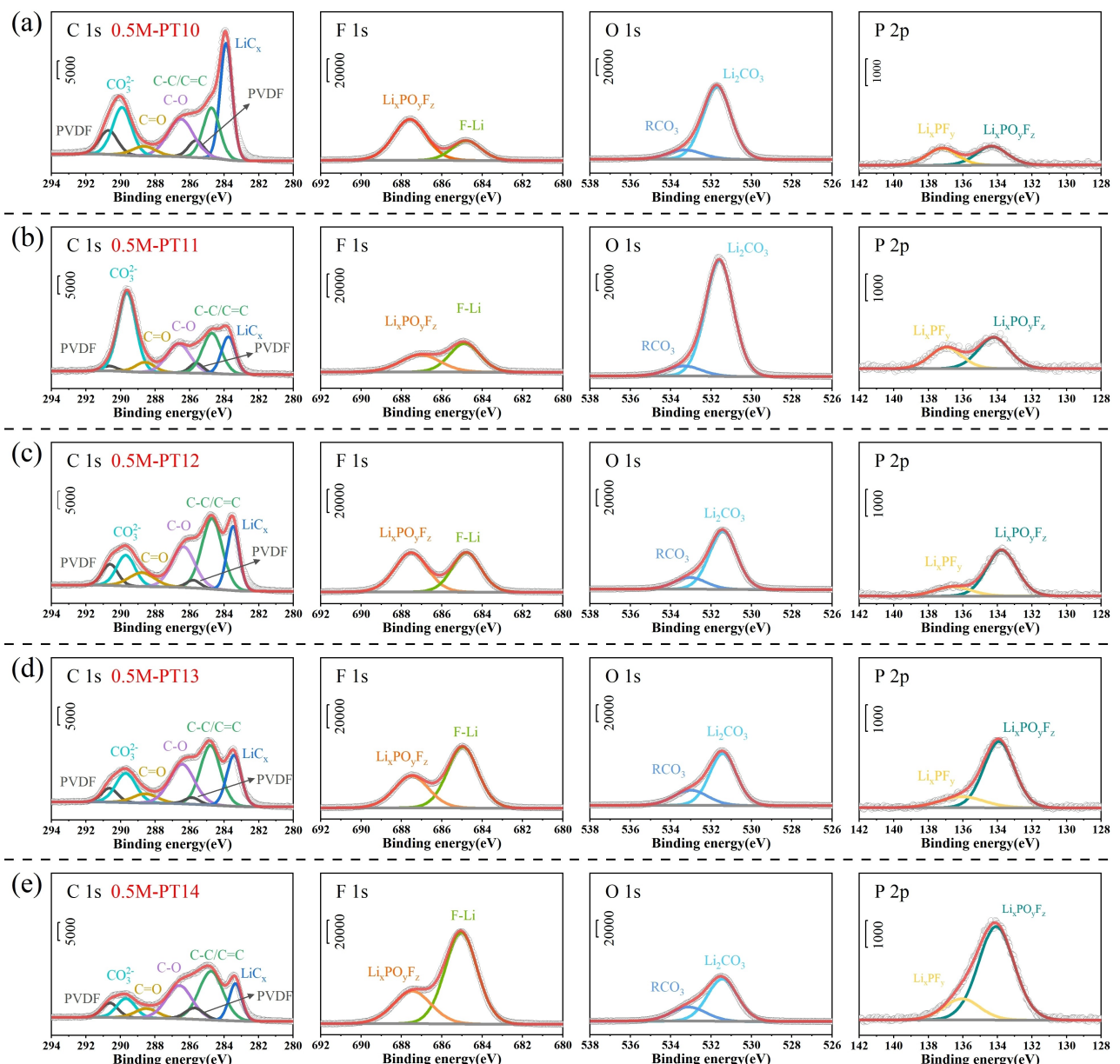


Figure 3. XPS analysis for the graphite anodes after one cycle in a) 0.5 M-PT10, b) 0.5 M-PT11, c) 0.5 M-PT12, d) 0.5 M-PT13 and e) 0.5 M-PT14 electrolyte.

after one cycle are thin. However, the peak intensities of LiC_x drop gradually, suggesting that the SEIs on the graphite anodes gets thicker with the addition of TTE.^[21] The relative contents of species containing CO_3^{2-} (289.7 eV), such as lithium carbonates (Li_2CO_3), continue to decline with the increase of TTE contents.^[22] It suggests the decomposition of PC is suppressed effectively. The atomic ratios of F and P elements on the graphite anodes keep increasing with the increase of TTE contents, indicating that more PF_6^- are reduced on the graphite anodes. The F 1s and P 2p spectra (Figure 3) show that the relative contents of LiF (684.8 eV) and $\text{Li}_x\text{PO}_y\text{F}_z$ (133.8 eV) keep increasing as the TTE contents increases.^[18,23,24] The results suggest the PF_6^- is much easier to reach the graphite anode surface to decompose to form an SEI rich in LiF and $\text{Li}_x\text{PO}_y\text{F}_z$ after the addition of TTE. It has been proved that a LiF-riched

SEI is conducive to strengthening the stability of the graphite interface.^[12] More importantly, it reveals that the Li^+ -solvation structure in the PC-based electrolyte directly determines the compositions of SEI on the graphite anode.

The cycle and rate performance of the $\text{Li} \parallel \text{graphite}$ cells in the 05PT system were accessed by typical charge/discharge tests. The electrolyte containing 1 M LiPF_6 in EC/DMC (3:7, V/V), abbreviated as 1 M-ED37, is used as a standard electrolyte. The $\text{Li} \parallel \text{graphite}$ cells in the 0.5 M-PT12, 0.5 M-PT13, and 0.5 M-PT14 electrolyte exhibit excellent cycling performances with almost no capacity loss for 50 cycles at 0.1 C (Figure 4). In contrast, the $\text{Li} \parallel \text{graphite}$ cell in the 1 M-ED37 electrolyte shows apparent fading in charge capacity. The SEM images (Figure S3) of graphite anodes after 50 cycles in the 05PT system and 1 M-ED37 electrolytes indicate that all graphite

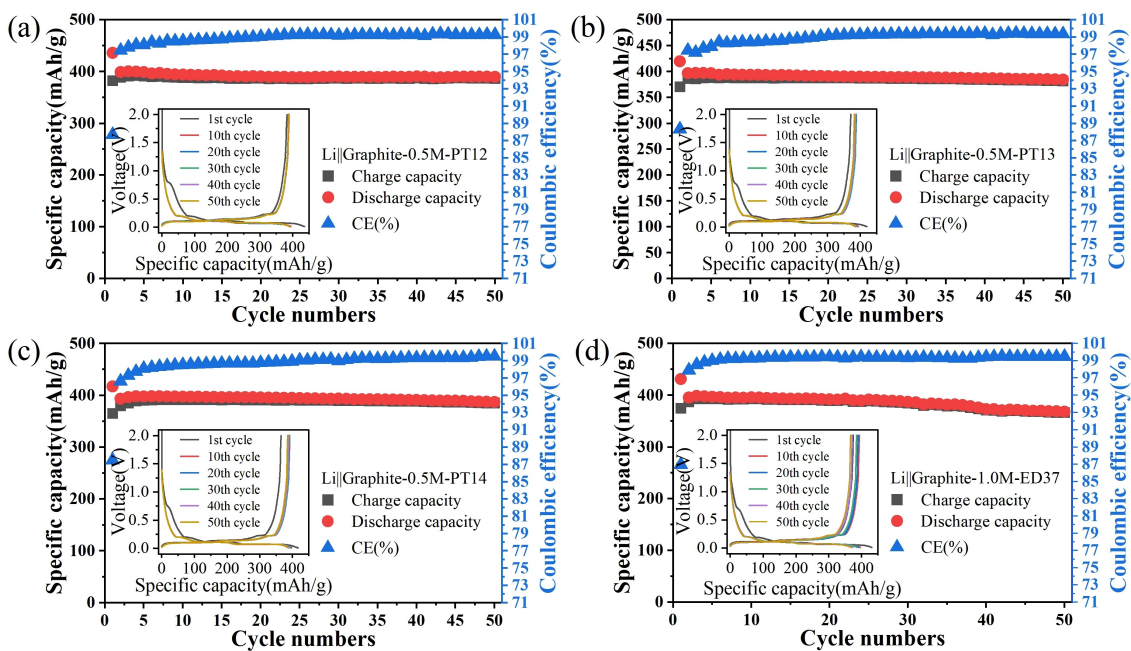


Figure 4. Cycling performances of $\text{Li}||\text{graphite}$ cells at 0.1 C in the a) 0.5 M-PT12 , b) 0.5 M-PT13 , c) 0.5 M-PT14 and d) 1 M-ED37 electrolyte. The insets are the corresponding charge/discharge profiles of $\text{Li}||\text{graphite}$ cells at 0.1 C .

particles maintain their initial shapes. The particle surfaces become rough due to the accumulation of electrolyte decomposition products. The Raman spectra (Figure S4) of the cycled graphite anodes indicate that the graphite's structure is well maintained. With the increase of TTE contents, the atomic ratios of F and P keep increasing, while the atomic ratios of C and O keep decreasing (Figure S5). In all electrolytes, the peak intensities of LiC_x in the C1s spectra reduce after 50 cycles because the SEIs get thicker during cycling.^[21] The relative contents of LiF and $\text{Li}_x\text{PO}_y\text{F}_z$ on the graphite surfaces keep increasing, while the species containing CO_3^{2-} keep decreasing (Figure S6). However, the graphite cycled in the 1 M-ED37 electrolyte exhibits low content of LiF and $\text{Li}_x\text{PO}_y\text{F}_z$ and high content of species containing CO_3^{2-} . The $\text{Li}||\text{graphite}$ cells in the 0.5 M-PT12 , 0.5 M-PT13 , and 0.5 M-PT14 electrolyte also display excellent cycling stabilities when charged and discharged at 0.2 C (Figure S7). The capacity retentions of $\text{Li}||\text{graphite}$ cells in the 0.5 M-PT12 , 0.5 M-PT13 , and 0.5 M-PT14 at 0.2 C are 95.2% , 94.7% , and 100% , respectively. When discharging at 0.2 C , the charge capacities of $\text{Li}||\text{graphite}$ cells in all electrolytes almost have no decline with the increase of charging rates from 0.2 C to 5 C (Figure S8). However, the fast-charging performances of the $\text{Li}||\text{graphite}$ cells in the 0.5 M-PT12 , 0.5 M-PT13 , and 0.5 M-PT14 electrolyte are slightly poor than that in the 1 M-ED37 electrolyte.

To confirm it's the change of Li^+ -solvation structures in the 05PT system rather than the volume ratios of PC to TTE that leads to the different electrochemical behaviors of $\text{Li}||\text{graphite}$ cells, we fixed the volume ratio of PC to TTE at $1:1$ and varied the concentration of LiPF_6 . The electrolyte formulas and identifications of the $x\text{mol LiPF}_6\text{-PC/TTE}(1:1, \text{V/V})$ system (PT11 system) are listed in Table 2. The Raman spectra (Figure 5a)

Table 2. Electrolyte formulas of the PT11 system.

Electrolyte formula	ID
$0.75 \text{ M LiPF}_6\text{-PC/TTE (1:1, V/V)}$	0.75 M-PT11
$1 \text{ M LiPF}_6\text{-PC/TTE (1:1, V/V)}$	1 M-PT11
$1.25 \text{ M LiPF}_6\text{-PC/TTE (1:1, V/V)}$	1.25 M-PT11

show that the increase of LiPF_6 concentrations in the PT11 system has similar influences as the increase of TTE contents in the 05PT system. The result validates that the addition of TTE in the 05PT system increases the localized concentration of Li^+ in the electrolyte.

We have known that the 0.5 M-PT11 electrolyte cannot suppress PC co-intercalation and continued electrolyte decomposition. Although the $\text{Li}||\text{graphite}$ cell in the 0.75 M-PT11 electrolyte still exhibits an extended platform near 0.8 V during the first discharge process, Li^+ successfully intercalates into the graphite anode to form a multi-stage Li_xC at last (Figure 5b). With the further increase of lithium salt concentration, the $\text{Li}||\text{graphite}$ cells in the 1 M-PT11 and 1.25 M-PT11 electrolyte display reversible (de)intercalation of Li^+ with no co-intercalation of PC molecules and persistent decomposition of electrolyte (Figures 5c and d, S9b and c). The initial charge capacity of the $\text{Li}||\text{graphite}$ cell in the 0.75 M-PT11 electrolyte at 0.1 C is 351.0 mAh g^{-1} , slightly lower than in the 1 M-PT11 (385.3 mAh g^{-1}) and 1.25 M-PT11 electrolyte (382.1 mAh g^{-1}). It indicates that a small number of PC molecules intercalate into the graphite anode in the 0.75 M-PT11 electrolyte. Besides, a broad cathodic peak near 0.8 V appears in the first cycle of the cyclic voltammogram for the $\text{Li}||\text{graphite}$ cell in the 0.75 M-PT11 electrolyte (Figure S9a), which can be ascribed to the co-intercalation of PC molecules and the violent decomposition of

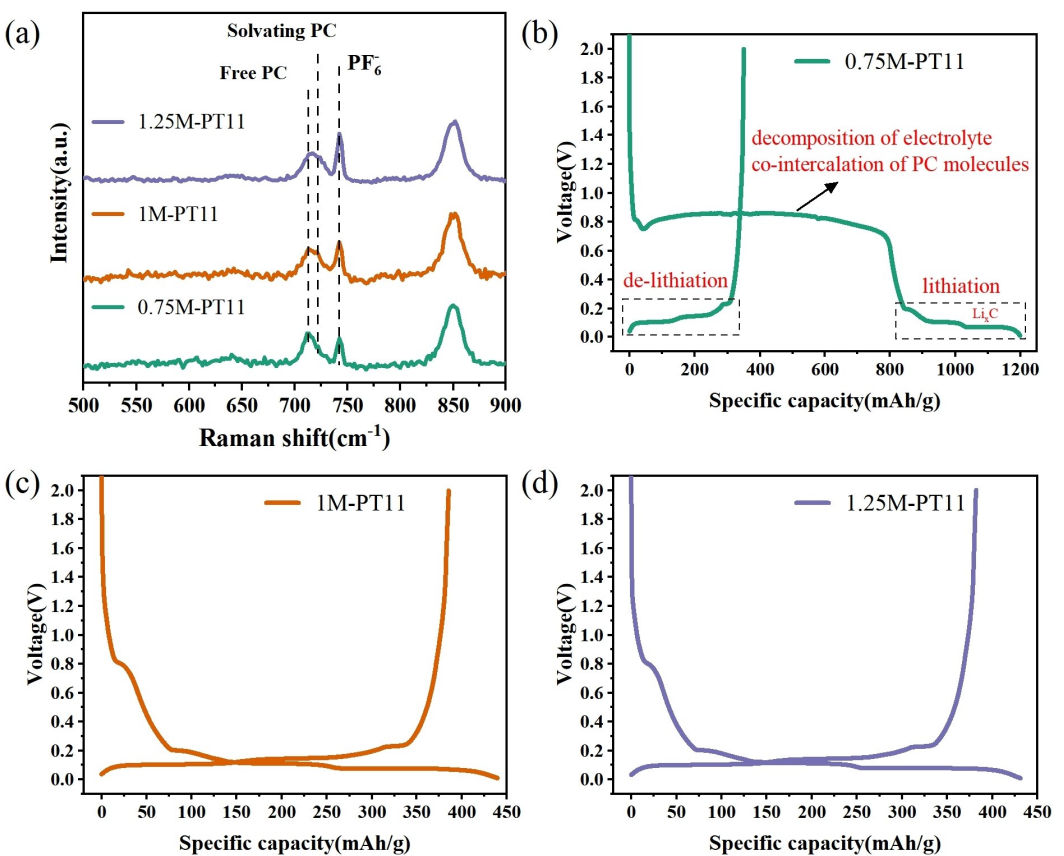


Figure 5. a) Raman spectra of the 0.75 M-PT11, 1.0 M-PT11, and 1.25 M-PT11 electrolyte. b-d) Initial voltage profiles of Li||graphite cells in the b) 0.75 M-PT11, c) 1.0 M-PT11, and d) 1.25 M-PT11 electrolyte at 0.1 C.

electrolyte. The cathodic peak disappears in the subsequent two cycles, indicating that an effective SEI is formed in the first cycle.

The SEM images (Figure S10) and Raman spectrum (Figure S11) of graphite anode after one cycle in the 0.75 M-PT11 electrolyte prove the co-intercalation of PC molecules. Notably, the graphite anode after one cycle in the 0.75 M-PT11 electrolyte has fewer tiny cracks than in the 0.5 M-PT11 electrolyte (Figure 2b). It indicates that fewer PC molecules co-intercalate into the graphite anode in the 0.75 M-PT11 electrolyte than in the 0.5 M-PT11 electrolyte. The 0.75 M-PT11 electrolyte failed to inhibit the co-intercalation of PC and decomposition of electrolyte in the beginning but succeeded in the end. It can be contributed to an effective SEI finally forming on the surface of the graphite anode. In addition, although the initial charge capacity of the Li||graphite cell in the 0.75 M-PT11 electrolyte at 0.2 C is only 333.9 mAh g⁻¹, the capacity retention after 100 cycles is as high as 99.6% (Figure S12). It suggests that part of graphite lost the ability to accommodate the (de)intercalation of Li⁺ due to the destruction of PC co-intercalation. However, the remaining graphite still has excellent stability to realize (de)lithiation.

To further validate the feasibility of this strategy to develop LCPEs for graphite anodes by manipulating the Li⁺-solvation structure, we used HFE to replace TTE in the LCPEs. The formula and identification for each electrolyte in the 0.5 M LiPF₆-PC/HFE

system (05PH system) are listed in Table 3. The Raman spectra (Figure 6a) reveal that the addition of HFE has the same effect as TTE: reinforcing the interaction between PC molecules/PF₆⁻ and Li⁺ and reducing the amount of free-state PC molecules. The Li||graphite cells in the 0.5 M-PH11 and 0.5 M-PH12 electrolyte display severe co-intercalation of PC molecules and sustaining decomposition of electrolyte (Figure 6b); the Li||graphite cells in the 0.5 M-PH13 and 0.5 M-PH14 electrolyte exhibit reversible (de)intercalation of Li⁺ (Figure 6c). The peak intensities of the cathodic peaks near 0.8 V keep decreasing with the increase of HFE contents, indicating the gradually enhanced suppression of PC decomposition (Figure S13).

The SEM images (Figure S14) and Raman spectra (Figure S15) of graphite anodes after one cycle confirm that the 0.5 M-PH13 and 0.5 M-PH14 electrolyte prevent the co-intercalation of PC molecules within graphite anodes while the 0.5 M-PH11 and 0.5 M-PH12 electrolyte fail. XPS measurement was also applied to check out the chemical compositions of the SEIs

Table 3. Electrolyte formulas of the 05PH system.

Electrolyte formula	ID
0.5 M LiPF ₆ -PC/HFE (1:1, V/V)	0.5 M-PH11
0.5 M LiPF ₆ -PC/HFE (1:2, V/V)	0.5 M-PH12
0.5 M LiPF ₆ -PC/HFE (1:3, V/V)	0.5 M-PH13
0.5 M LiPF ₆ -PC/HFE (1:4, V/V)	0.5 M-PH14

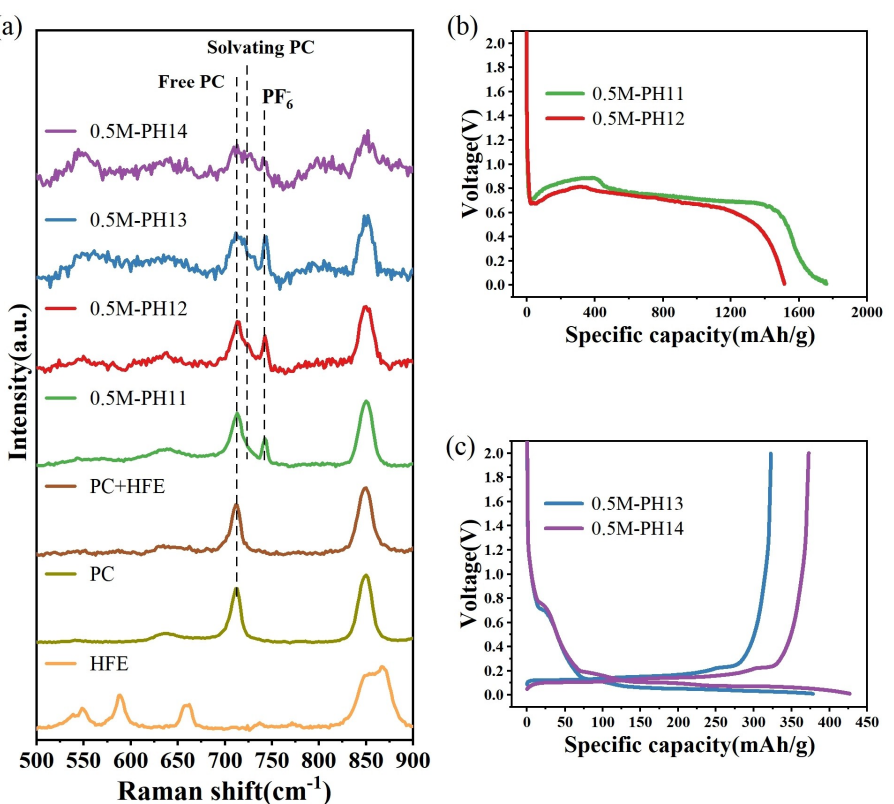


Figure 6. a) Raman spectra of HFE, PC, PC+HFE, 0.5 M-PH11, 0.5 M-PH12, 0.5 M-PH13, and 0.5 M-PH14. b) Initial voltage profiles of $\text{Li}||\text{graphite}$ cells in the 0.5 M-PH11 and 0.5 M-PH12 electrolyte at 0.1 C. c) Initial voltage profiles of $\text{Li}||\text{graphite}$ cells in the 0.5 M-PH13 and 0.5 M-PH14 electrolyte at 0.1 C.

on graphite anodes after one cycle in the 0.5 M-PH11, 0.5 M-PH12, 0.5 M-PH13, and 0.5 M-PH14 electrolyte (Figure S16 and S17). The results are highly consistent with the XPS data of graphite anodes after one cycle in the 05PT electrolyte system. It demonstrates that HFE plays a similar role to TTE in the LCPEs.

Conclusion

In summary, we achieved highly reversible (de)intercalation of Li^+ within graphite anodes in LCPEs by manipulating the Li^+ -solvation structures with inert cosolvents (TTE/HFE) unprecedentedly. We found that the relative contents of LiF and $\text{Li}_x\text{PO}_y\text{F}_z$ derived from PF_6^- on the cycled graphite anodes keep increasing with the increase of TTE (or HFE) contents in the LCPEs, indicating more PF_6^- are decomposed on the graphite anodes to form anion-derived SEIs. It proves that the Li^+ -solvation structure directly determines the compositions of the SEI. More importantly, this work demonstrates the feasibility of obtaining a LiF-riched SEI on the graphite anode in LCPE by manipulating the Li^+ -solvation structure with inert cosolvent. The LiF-riched SEI prevents PC molecules co-intercalation and electrolyte decomposition effectively. We believe our results are significant for revealing that interfacial stability is strongly dependent on the Li^+ -solvation structure in PC-based electrolyte and providing new insights for developing promising

electrolytes based on the Li^+ -solvation structures for next-generation LIBs.

Experimental Section

Materials. Battery-grade LiPF_6 , propylene carbonate (PC), ethylene carbonate (EC), dimethyl carbonate (DMC), 1,1,2,2-tetrafluoroethyl-2,2,3,3-tetrafluoropropylether (TTE) and 1,1,2,2-tetrafluoroethyl-2,2,2-trifluoroethyl ether (HFE) were purchased from Aladdin Industrial Corporation. Graphite was kindly supplied by BTR New Material Group Co., Ltd. Li chips (500 μm , area 1.77 cm^2) were purchased from China Energy Lithium Co., Ltd.

Electrolyte preparation and characterization. All the electrolytes were prepared in an Ar-filled glovebox (MIKROUNA). The solution structures of the LCPEs were characterized by Raman spectroscopy (Renishaw InVia Reflex, England).

Electrochemical performances measurements. The graphite anode composition was 80 wt% graphite, 10 wt% acetylene black, and 10 wt% polyvinylidene fluoride (PVDF). The active materials loading is $\sim 1.5 \text{ mg cm}^{-2}$. Galvanostatic charge/discharge cycling were assessed using CR2025-type cells with a cutoff voltage between 0.01–2 V by the Neware battery test system (BTS9000, Shenzhen, China) and Land battery test system (BT2001, Wuhan, China) at room temperature. Cyclic voltammograms were performed with an Electrochemical Workstation (DongHua Test, DH7000, Jiangsu) at a sweep rate of 0.1 mV s^{-1} .

Material characterization. The morphologies of pristine and cycled graphite anodes were obtained by scanning electron microscope

(SEM, TESCAN MIRA LMS). The graphitization degree of the graphite anodes was measured by Raman spectroscopy (Renishaw InVia Reflex, England). The surface components of cycled graphite anodes were examined by X-ray photoelectron spectroscopy (Thermo Scientific K-Alpha⁺).

Acknowledgements

This work was supported by the National Natural Science Foundation of China (51772333 and 51874358). The authors would like to appreciate the help of XPS tests from Shiyanjia Lab (www.shiyanjia.com).

Conflict of Interest

The authors declare no conflict of interest.

Data Availability Statement

The data that support the findings of this study are available from the corresponding author upon reasonable request.

Keywords: graphite anode · interfacial stability · lithium⁺-solvation structure · low concentration · propylene carbonate-based electrolyte

- [1] K. Xu, *Chem. Rev.* **2004**, *104*, 4303–4418.
- [2] K. Xu, *Nat. Energy* **2021**, *6*, 763–763.
- [3] D. Aurbach, K. Gamolsky, B. Markovsky, Y. Gofer, M. Schmidt, U. Heider, *Electrochim. Acta* **2002**, *47*, 1423–1439.
- [4] W. Yao, Z. Zhang, J. Gao, J. Li, J. Xu, Z. Wang, Y. Yang, *Energy Environ. Sci.* **2009**, *2*, 1102.

- [5] B. Li, M. Xu, T. Li, W. Li, S. Hu, *Electrochim. Commun.* **2012**, *17*, 92–95.
- [6] K. Wang, L. Xing, H. Zhi, Y. Cai, Z. Yan, D. Cai, H. Zhou, W. Li, *Electrochim. Acta* **2018**, *262*, 226–232.
- [7] L. J. Fu, J. Gao, T. Zhang, Q. Cao, L. C. Yang, Y. P. Wu, R. Holze, *J. Power Sources* **2007**, *171*, 904–907.
- [8] J. Gao, L. J. Fu, H. P. Zhang, L. C. Yang, Y. P. Wu, *Electrochim. Acta* **2008**, *53*, 2376–2379.
- [9] L. C. Yang, W. L. Guo, Y. Shi, Y. P. Wu, *J. Alloys Compd.* **2010**, *501*, 218–220.
- [10] S.-K. Jeong, M. Inaba, Y. Iriyama, T. Abe, Z. Ogumi, *Electrochim. Solid-State Lett.* **2003**, *6*, A13.
- [11] S.-K. Jeong, M. Inaba, Y. Iriyama, T. Abe, Z. Ogumi, *J. Power Sources* **2008**, *175*, 540–546.
- [12] M. Nie, D. P. Abraham, D. M. Seo, Y. Chen, A. Bose, B. L. Lucht, *J. Phys. Chem. C* **2013**, *117*, 25381–25389.
- [13] M. Zhang, J. Zhang, J. Yang, J. Yao, Z. Chen, C. Lu, X. Du, Z. Zhang, H. Zhang, G. Cui, *Chem. Commun.* **2019**, *55*, 9785–9788.
- [14] D. Guan, G. Hu, Z. Peng, Y. Cao, J. Wu, M. Huang, S. Zhang, Y. Dai, Y. Gong, K. Du, *J. Mater. Chem. A* **2022**, *10*, 12575–12587.
- [15] Y.-S. Kim, S.-K. Jeong, *J. Spectrosc.* **2015**, *2015*, 1–5.
- [16] H.-Y. Song, M.-H. Jung, S.-K. Jeong, *Appl. Sci.* **2019**, *9*, 4647.
- [17] T. Doi, R. Masuhara, M. Hashinokuchi, Y. Shimizu, M. Inaba, *Electrochim. Acta* **2016**, *209*, 219–224.
- [18] X. Liu, X. Shen, H. Li, P. Li, L. Luo, H. Fan, X. Feng, W. Chen, X. Ai, H. Yang, Y. Cao, *Adv. Energy Mater.* **2021**, *11*, 2003905.
- [19] S. Maruyama, T. Fukutsuka, K. Miyazaki, Y. Abe, N. Yoshizawa, T. Abe, *J. Electrochem. Soc.* **2018**, *165*, A2247–A2254.
- [20] Y. Wang, Y. Zhang, S. Wang, S. Dong, C. Dang, W. Hu, D. Y. W. Yu, *Adv. Funct. Mater.* **2021**, *31*, 2102360.
- [21] M. Khasanov, E. Pazhetnov, W. C. Shin, *J. Electrochem. Soc.* **2015**, *162*, A1892–A1898.
- [22] X.-G. Sun, C. Liao, L. Baggetto, B. Guo, R. R. Unocic, G. M. Veith, S. Dai, *J. Mater. Chem. A* **2014**, *2*, 7606–7614.
- [23] P. Murmann, P. Niehoff, R. Schmitz, S. Nowak, H. Gores, N. Ignatiev, P. Sartori, M. Winter, R. Schmitz, *Electrochim. Acta* **2013**, *114*, 658–666.
- [24] B. Li, M. Xu, B. Li, Y. Liu, L. Yang, W. Li, S. Hu, *Electrochim. Acta* **2013**, *105*, 1–6.

Manuscript received: June 7, 2022
Revised manuscript received: July 15, 2022
Accepted manuscript online: July 19, 2022
Version of record online: August 3, 2022